Chemical and Physical Transformations of Silver Nanomaterial Containing Textiles After Modeled Human Exposure

Danielle E Gorka*, Nancy J. Lin, John M. Pettibone, Justin M Gorham*

National Institute of Standards and Technology, 100 Bureau Drive, Gaithersburg, MD, USA 20899

*danielle.gorka@nist.gov; justin.gorham@nist.gov

For submission to NanoImpact

Abstract

The antimicrobial properties of silver nanomaterials (AgNM) have been exploited in various consumer applications, including textiles such as wound dressings. Understanding how these materials chemically transform throughout their use is necessary to predict their efficacy during use and their behavior after disposal. The aim of this work was to evaluate chemical and physical transformations to a commercial AgNM-containing wound dressing during modeled human exposure to synthetic sweat (SW) or simulated wound fluid (WF). Scanning electron microscopy with energy dispersive X-ray spectroscopy (EDS) revealed the formation of micrometer-sized structures at the wound dressing surface after SW exposure while WF resulted in a largely featureless surface. Measurements by X-ray photoelectron spectroscopy (XPS) revealed a AgCl surface (consistent with EDS) while X-ray diffraction (XRD) found a mixture of zero valent silver and AgCl suggesting the AgNM wound dressings surface formed a passivating AgCl surface layer after SW and WF exposure. For WF, XPS based findings revealed the addition of an adsorbed protein layer based on the nitrogen marker which adsorbed released silver at prolonged exposures. Silver release was evaluated by inductively coupled plasma mass spectrometry which revealed a significant released silver fraction in WF and minimal released silver in SW. Analysis suggests that the protein in WF sequestered a fraction of the released silver which continued with exposure time, suggesting additional processing at the wound dressing surface even after the initial transformation to AgCl. To evaluate the impact on antimicrobial efficacy, zone of inhibition (ZOI) testing was conducted which found no significant change after modeled human exposure compared to the pristine wound dressing. The results presented here suggest AgNM-containing wound dressings transform chemically in simulated human fluids resulting in a material with comparable antimicrobial properties with pristine wound dressings. Ultimately, knowing the resulting chemical properties of the AgNM wound dressings will allow better predictive models to be developed regarding their fate.

Keywords: silver nanomaterials, textile, wound dressings, characterization, antimicrobial

1. Introduction

Nanomaterials have been increasingly incorporated into new and existing consumer products due to their unique and improved properties over the past 2 decades. Silver nanomaterials (AgNMs) have been used in many applications for their antimicrobial properties.[1] Consumer textiles such as athletic clothing, socks, and stuffed animals incorporate AgNMs to prevent microbial growth and odors.[2-4] Additionally, AgNMs are found in biomedical products such as creams, catheters, bandages, and wound dressings as a preventative measure against infections.[5] Clearly, silver as a nano-additive has a significant footprint as an antimicrobial agent in select applications.

AgNM-containing textiles make up a large share of the different silver enabled consumer products. To understand how these materials will impact their surroundings, it is important to know how they transform while in use, not only in physical and elemental composition terms, but also chemically (e.g. $Ag^0 \rightarrow AgCl$). A significant body of work currently exists regarding the silver released from exposing AgNM-containing textiles (*e.g.* socks, shirts, underwear, etc.) to various simulated fluids (*eg* sweat, wound fluid, washing solutions).[6-14] For example, several studies have determined synthetic sweat caused release of released silver species (*e.g.* soluble $AgCl_x$ complexes) from AgNM textiles where many of the silver cations would precipitate into AgCl under the high $[Cl^-]$.[9, 11] In other sweat exposure studies, there is some elemental evidence suggesting the transformed AgCl deposits back onto the textiles, and the remaining soluble silver species in solution has been predicted to be $AgCl_x$ [10]. Additionally, Kulthong et al. found the amount of silver released from laboratory-prepared AgNM-containing textiles increases with increasing silver content.[7] These studies are all consistent with previous work by Liu et al. who demonstrated an equilibrium of silver species forming depending on the starting $[Ag^+]$ and $[Cl^-]$ ratios[15]. In concert, these findings verify that the AgNM-containing textiles exposed to sweat will release silver (e.g. $AgCl_x$ (*aq*)), yet also have some of it redeposited as a complex on the textile surface (*e.g.* AgCl, etc.). Furthermore, $AgCl_x$ compounds have been demonstrated to be antimicrobial which suggests that sweat exposure may not eliminate this beneficial property [16-18].

Within the textile 'class' of materials, there are also bandages that possess a nanosilver component and are commonly used for wounds, specifically burns [8, 19]. These wound dressings have been studied as well to understand the impact of their physical and elemental properties upon exposure to sweat. Fewer studies have focused on the chemical transformations of the AgNM-containing wound dressing itself. [8, 20-23] The existing data suggests that these materials will also release silver when exposed to simulated sweat and are likely to complex into AgCl species [6, 8] Recent studies suggest that only a small (i.e. not statistically significant) amount of the silver is released from wound dressings during use.[24] Therefore, the majority of the silver will remain on the product upon disposal where, based on additional studies, there is a potential for environmental consequences.[25-27] One possible endpoint is for these materials to end up in a landfill. In a model landfill scenario, AgNMs were found to inhibit the anaerobic digestion of waste in a bioreactor, decreasing the number of methanogenic species.[28, 29] For

these studies and other disposal scenarios, knowledge of the AgNMs' chemical composition would have assisted in predicting potentially negative environmental phenomena since released silver, which is greatly impacted by the chemical state, is likely the cause of the aforementioned antimicrobial behavior. However, to the authors knowledge most studies focus largely on the elemental and physical changes that occur to the AgNM enabled wound dressings and interpret chemical states based on that information rather than directly probe the distribution of silver species. To better understand the wound dressings chemical transformations while in use, this study will focus on the chemical transformations that occur to wound dressings during use. Evaluation of silver release and antimicrobial efficacy will also be measured and compared to previous reports.

The focus of this manuscript was to understand the chemical distribution of silver species throughout the surface and bulk of an AgNM enabled wound dressing, and to understand how that distribution changes as a function of simulated use. After verification of the presence of silver on the wound dressing surface, silver speciation and other physical/elemental properties were evaluated before and after exposure to synthetic sweat (SW) and simulated wound fluid (WF). Samples were characterized by electron microscopy and X-ray spectroscopy for physical and elemental analysis, respectively, while X-ray diffraction (XRD) and X-ray photoelectron spectroscopy (XPS) were employed to evaluate chemical transformations. To compare our findings with previously reported work, inductively coupled plasma – mass spectrometry (ICP-MS) was also employed to evaluate silver release and quantify silver loading, while the impacts of chemical transformations on the wound dressing's antimicrobial properties were evaluated by zone of inhibition (ZOI).

2. Materials and Methods[1]

2.1 Wound dressing and exposure

The commercial wound dressing we employed was advertised to consist of multiple layers of rayon, polyethylene and silver coatings. Three of the five layers (first, third, and fifth) were composed of silver/ silver oxide deposited onto a high-density polyethylene mesh backing via sputtering processing (manufacturer's claim). The second and fourth layers were composed of a rayon/polyester gauze.

Test solutions (synthetic SW and simulated WF) were prepared to mimic human exposure during use. Synthetic SW was prepared following the International Standard Organization (ISO)105-E04-2008E acidic type synthetic SW method.[30] Briefly, 0.5 g l-histidine monochloride monohydrate (VWR, Radnor, PA, USA), 5 g sodium chloride (99 %, Alfa Aesar Haverhill, MA, USA), and 2.2 g sodium dihydrogen orthophosphate dihydrate (99 %, Alfa Aesar) were mixed and diluted to 1 L with 18 MΩ cm deionized (DI) water. Simulated WF

[1] Certain commercial entities, equipment, or materials may be identified in this document in order to describe an experimental procedure or concept adequately. Such identification is not intended to imply recommendation or endorsement by the National Institute of Standards and Technology, nor is it intended to imply that the entities, materials, or equipment are necessarily the best available for the purpose.

consisted of an isotonic solution with an added 1 % (by mass) protein component.[31] Briefly, 8.27 g sodium chloride (99%, Alfa Aesar,), 0.37 g calcium chloride dihydrate (Amresco), and 10 g bovine serum albumin (BSA, SeraCare, Milford, MA, USA) were mixed and diluted to 1 L with DI water. The pH values of the pristine synthetic SW and simulated WF solutions were 4.36 and 6.91, respectively.

An approximately 17 mm by 17 mm (2/3 inch by 2/3 inch) piece of the complete wound dressing was fully submerged in 10 mL of test solution in a 30 mL low density polyethylene bottle. The bottle was foil wrapped to prevent light exposure and rotated horizontally on a shaker (Barnstead MaxQ 4000, Thermo Fisher, Waltham, MA, USA) at 50 rpm at room temperature. The wound dressing was removed at the following times after addition: 5 s, 1 h, 2 h, 6 h, 24 h, and 168 h. 168 h was chosen since it is the manufacturer's and FDA recommended device lifetime. The wound dressing was stored in a vacuum desiccator while the test solution was stored in the dark at 4 °C. For each exposure and time point, a total of n = 3 wound dressing samples were exposed in separate starting test solutions.

2.2 Characterization

The pristine wound dressing was first examined to ensure that the manufacturer's claims were accurate. For characterization of the pristine and exposed wound dressings, the middle silver-containing layer was used for characterization to minimize potential contamination of the outer layers unless otherwise mentioned. Wound dressings (both pristine and exposed) were analyzed by scanning electron microscopy (SEM) with energy-dispersive X-ray spectroscopy (EDS) using a FEI Quanta 200 (Hillsboro, OR) microscope and a Bruker XFlash EDS Detector 5030 (Billerica, MA). Samples were prepared by adding a small segment of wound dressing (≈ 2 mm x 2 mm) to an aluminum stub with carbon tape. Sample preparation for a cross-sectional image of the surface was conducted by affixing the wound dressing to a 90 degree stub and cutting an edge with scissors. Samples were imaged at an operating voltage of 10 kV. For EDS maps and spectra, an acquisition time of 300 s was used. EDS data were analyzed using Bruker Esprit v. 1.9.3 software. Wound dressing particle size was determined using ImageJ software (National Institutes of Health, Bethesda, MD). Over 500 individual nanoparticles were manually measured from 7 images of 1 wound dressing sample, with size reported as mean ± one standard deviation. In this manuscript, standard deviations serve to represent the standard uncertainty associated with the measurements. The pH of the test solutions was measured with an Orion 2 Star (Thermo Scientific, Waltham, MA) using a Mettler Toledo model InLab semi-micro pH electrode with NIST traceable buffers. The samples were kept in a vacuum desiccator in minimal light until characterization could occur.

XPS was carried out using an Axis Ultra DLD spectrophotometer from Kratos Analytical (Chestnut Ridge, NY). Samples were mounted *ex-situ* onto a sample bar with carbon tape and fastened on at least one side with a metal strap to dissipate charging. For controls, a sputtered clean (4 kV argon ions) silver foil specimen, silver oxide and a silver chloride powder were employed. Sample bars were loaded and pumped down prior to entrance into high vacuum conditions, or P_{base} = 2.7 x 10^{-7} Pa (P_{base} = 2 x 10^{-9} torr). Photoemission was achieved by exposure of the samples to monochromatic Al Kα X-rays, and ejected electrons were collected

along the surface normal from an area defined by FOV1 lens and a 110 µm aperture (≈ 190 µm diameter). Photoelectrons were analyzed at pass energy 40 eV and a 0.1 eV step size for different times depending upon the element's concentration and relative sensitivity factors (RSF). Though sodium and silicon were detected in all exposed samples, they are not discussed in the manuscript. For each condition, the values provided are representative of the average ± one standard deviation of 2 to 4 measurements of spatially unique regions on one sample. Spectra were processed using CasaXPS (Teignmouth, UK) with elemental RSF's provided specific to the Axis Ultra. For reference, the Ag $3d^5$ was set to 368.2 eV to more easily compare the wound dressings by monitoring chemical shifts in the Ag MNN feature. Assessment of silver's oxidation state was carried out by monitoring both the binding energy (BE) of the Ag $3d^{5/2}$ signal and the kinetic energy (KE) of the Ag MNN (letters correspond to the principal energy level, or electron shells, associated with the Auger process) using the below equation for modified Auger parameters (α') [32]:

$$\alpha' = BE_{Ag\ 3d5/2} + KE_{Ag\ MNN}$$

α' was employed because variability in the photoelectron peak position for silver metal (Ag^0) and silver chloride (AgCl) is minor (≤ 0.3 eV). There were several issues associated with charging and X-ray induced modifications that were minimized to the best abilities of the authors, however these also eliminated our ability to use the C 1s spectra. For further information on these issues and background assignment and fitting, please refer to the SI.

Samples were analyzed for their crystallinity by XRD using a Bruker D8 Discover X-ray diffractometer with a VANTEC500 detector. The X-ray source was Cu Kα at 40 kV and 40 mA, with a 1 mm collimating pinhole and snout. Each measurement consisted of three, 25° 2 θ segments from 15° 2 θ to 90° 2 θ, where data for each segment was collected for 300 s. Samples were analyzed using DIFFRAC.SUITE EVA (Bruker). For each sample from each of the three trials, an approximately 5 mm x 5 mm piece of the wound dressing was attached to the XRD stage using carbon tape. Three measurements were taken for each sample at unique positions on the wound dressing.

The silver released into the exposure media was analyzed using an Agilent 7900 ICP-MS (Santa Clara, CA). Samples were prepared by undergoing digestion in 1% (by volume) nitric acid (Fischer Scientific Optima) overnight. Samples were not filtered before analysis and as such would include any silver ions, soluble silver species, and silver nanoparticles that were released during exposure. Samples were introduced into the ICP torch using an Agilent MicroMist nebulizer and an impact bead spray chamber cooled to 2 °C. The instrument was tuned daily for 1 µg/L (ppb) Li, Y, and Yb (Agilent, ICP-MS PA tuning solution). The RF power was 1550 W. Carrier gas had a flow of 1.05 L min^{-1}. Each measurement consisted of 5 replicates, with each replicate consisting of 100 sweeps and an integration time of 1 s. Calibration standards were measured daily at the start of the run, as well as every 18 samples to detect drift. Calibration standards were prepared using NIST Standard Reference Material (SRM) 3151 Silver Standard Solution in 1 % (by volume) nitric acid (Fisher Scientific Optima). Exposure media solutions were prepared by dilution in 1 % (by volume) nitric acid (Fisher Scientific Optima) and digesting

overnight. The exposure media from each trial was run once. The value reported is the mean ± one standard deviation of the three separate trials.

Lastly, the mass fraction of silver in the wound dressing was measured using ICP-MS. Three separate specimens (17.8 mm x 17.8 mm) were cut from three separate packages of wound dressing and the total mass was measured using a ML54 balance by Mettler Toledo (Columbus, OH). From each specimen, three samples were cut and their individual mass was measured and placed into clean LDPE bottles. 0.005 L of DI water and 0.01 L of 70% HNO_3 (Fisher Chemical, OPTIMA grade) were added to the bottle sequentially. The solution was allowed to react for at least 75 min. The samples were diluted in > 2% HNO_3 solution containing 1 ug L^{-1} Pd as an internal standard, where the *m/z* 105 was monitored. The ICP-MS conditions previously reported for all release experiments were used for total Ag measurements.

2.3 Zone of Inhibition Testing

To determine if exposure to SW or WF affected the bacterial toxicity of the wound dressing, ZOI tests were performed using the bacteria *Staphylococcus aureus* and *Pseudomonas aeruginosa*. Three time-points for each exposure media were examined; 5 s to mimic minimal use, 24 h to mimic medium use, and 168 h to mimic the maximal recommended use of the commercial wound dressing. For ZOI tests, pieces of pristine and exposed wound dressing were cut from the exposed material using a standard hole punch (6 mm in diameter) and the middle layer of the wound dressing was used. Disks were cut from a new pack of Whatman 40 filter paper using a standard hole punch, and then autoclaved at 121 °C for 20 min to sterilize. To load the disks, 10 µL of test solution was placed onto each disk and allowed to dry in a biosafety cabinet. The test solutions used were pristine synthetic SW, pristine simulated WF, and exposed supernatant solutions at t = 5 s, 24 h, and 168 h for both SW and WF. To prepare the positive control disks (10 µg Ag^+), 10 µL of a 1000 mg/L Ag^+ (from silver nitrate, $AgNO_3$, Premion, Alfa Aesar) in DI water was placed on the disk and allowed to dry in a biosafety cabinet. Blank disks were used as negative controls.

Bacterial cultures (*S. aureus* ATCC 25923, *P. aeruginosa* ATCC 27853, American Type Culture Collection, Manassas, VA, USA) were grown 18 h in tryptic soy broth (TSB). The bacteria were then streaked onto TSB agar plates and incubated at 37 °C for 18 h. The streak plates were stored at 4 °C for up to two weeks. Approximately 5 colonies were taken from the streak plate and restreaked onto a fresh TBS agar plate and incubated at 37 °C for 23 h. Approximately 7 colonies were taken from the fresh streak plate and added to TSB to achieve an optical density at 600 nm (OD600) of 0.1. This cell suspension was used to inoculate TSB agar plates for ZOI testing. To prepare the plates, 100 µL of the bacteria (OD600 = 0.1) was spread onto the TSB agar plate using a sterile, disposable plastic spreader. The disks or wound dressing samples were placed evenly spaced on the plate, with the silver side down for wound dressing samples. The plates were incubated 24 h at 37 °C. Plates were imaged using a RevSci IncuCount Colony Counter (Revolutionary Science, Schafer, MN, USA). The ZOI was determined by measuring the cleared area using ImageJ based on previous reports and further described in the SI.[33] Statistical

analysis was performed using Orgin2018b (OriginLab Corp., Northhampton, MA, USA). A test for normality was performed before ANOVA and posthoc testing using Tukey HSD. Values are represented as mean zone of inhibition (n=9) ± one standard deviation. Different letters indicate statistical significance at p = 0.05.

3. Results

3.1 Chemical Characterization of the pristine wound dressing

Here, we evaluate the pristine wound dressing to better understand the initial chemical state of the AgNM as well as the physical and elemental properties. By visual inspection, the silver layers were a bluish color on one side (See SI Figure S1, left) and silver on the other. Evaluation of the pristine wound dressing's surface morphology using SEM/EDS revealed a nanostructured surface with spherical nanoparticles (Figure 1A and SI Figure S3A). Most of the nanoparticles present ranged between 10 nm and 25 nm in diameter, yielding an average of 17.7 nm ± 7.4 nm (n = 500). Inspection of a crude cross-section of the silver/polyethylene layer revealed the silver deposited on the surface was a contiguous film between 500 nm to 1 μm thick (SI Figure S4; thickness shown by red arrow). EDS analysis was performed in conjunction with SEM analysis. The pristine material (Figure 1A) consisted of predominantly silver signatures with some minor contributions from other low molecular weight elements such as carbon and oxygen. The presence of carbon is likely due to the polyethylene mesh support used on the wound dressing and the presence of oxygen can be attributed to the presence of silver oxide as described by the manufacturer. EDS mapping supported the notion that the silver surface was uniform in coverage. The measured mass fraction of silver (ICP-MS) in the wound dressing was (0.10 +/- 0.0059) g/g (m_{Ag}/m_{WD}) and the total silver in the 17 mm x 17 mm was calculated to be 5.3 mg +/- 0.41 mg.

Chemically, the pristine wound dressing was characterized by both XRD and XPS. XRD measurements were performed to determine the distribution of silver composition within the bulk of the wound dressings. XRD data for the pristine wound dressing (Figure 2) contained diffraction peaks consistent with predominantly zero-valent silver and silver oxide, which agreed with work by Taylor et al.[23] Further examination of the surface elemental and silver chemistry was conducted by XPS analysis. Figure 3 summarizes the findings in the form of stackplots of raw Ag *3d* and Cl *2p* spectra. The α' values gleaned from each sample set and control are presented in SI Table S1. For the pristine wound dressing, a α' value of 723.3 eV ± 0.1 eV was assigned, consistent with a silver (I) state. Previously reported α' values for silver oxide (Ag_2O) were between 724.2 eV and 724.4 eV [32] and our internal controls yielded a value at 723.8 eV. Both current sample values and controls are clearly shifted from our silver foil control, 726.1 eV ± 0.0 eV, but are also inconsistent with the literature values for silver oxide. Since XRD measurements indicate the presence of silver oxides (limit of detection 1%), the surface silver may have been in a different oxidized state consisting of more than one species. One potential complex may be silver carbonate (Ag_2CO_3) which has a comparable α' value at the surface with what we measured.[34] Regardless, we can be relatively certain that the observed Ag composition was not AgCl due to the lack of significant Cl *2p* peak intensity (Figure 4).

Combined, the data suggested that the AgNM layers of the pristine wound dressing composed of an oxidized surface layer over a predominantly Ag^0 film.

3.2 Transformations due to SW exposure

The chemical impacts of SW exposure were first observed for AgNM enabled wound dressings as a visibly apparent color change from blue (pristine material) to brown (exposed material) (SI Figure S1, center), which occurred after 168 h. Electron microscopy revealed a physical transformation of the pristine nanostructured surface to non-spherical crystals after SW exposure at t =168 h. The crystals were on the order of 100 nm to 200 nm in size and formed almost immediately upon SW exposure and grew up to several microns in length after 168 h (Figure 1B, SI Figure S3B and S3C). EDS results revealed that both silver (red) and chlorine (blue) were co-located on the surface, suggestive of a transformation to AgCl. Low Z elements were also detected, such as carbon and oxygen that were attributed to the backing, as well as sodium. In some instances, pitting was observed on the surface (SI Figure S5), which resulted in Cl poor regions, suggesting that this might be a drying artifact after removal from solution. In other regions, the pitting was observed and the AgNM layer was completely removed, demonstrated by the absence of silver and chlorine intensity in EDS maps (SI Figure S6). This was rarely observed and only in localized regions.

Chemically speaking, the surface transformed to predominantly AgCl after SW exposure, as observed through the XRD measurements. Indeed, the silver oxide peak in the XRD spectrum disappears completely after the wound dressing was exposed to synthetic SW (Figure 2A). Peaks for silver chloride appear in the SW-exposed spectra, consistent with EDS mapping, and suggest that the non-spherical crystals on the wound dressing were predominantly silver chloride. Interestingly, the wound dressing does not show complete transformation to silver chloride since the zero-valent silver peaks remain even after 168 h of SW exposure. This is consistent with some of the pitting imaged by EDS mapping which demonstrate the presence of silver and the absence of chlorine (SI Figure S5)

XPS also corroborated the presence of silver chloride using two different metrics. First, the surface chemically transformed to one consistent with the silver chloride control after exposure to SW, as evident by a shift in α' from 723.3 ± 0.1 eV to 723.6 ± 0.2 eV for the pristine AgNM wound dressing and 168 h SW treated wound dressing, respectively (Figure 3, SI Table S1). While the shift is quite small in terms of XPS, the value was reproducible and consistent with the silver chloride control, 723.5 ± 0.1 eV. From an elemental analysis standpoint, the Cl 2p peak also became readily apparent. Semiquantitative atomic ratio plots are presented in Figure 4 and are supported by representative stackplots for SW exposed AgNM wound dressing (Figure S7). The Cl:Ag ratio provides further evidence of the surface transformation to AgCl. This is evidenced by the sharp increase of Cl:Ag value from 0.039 ± 0.02 in the pristine wound dressing to an average value of 0.89 ± 0.04 for all measurements $\geq$ 6 h SW exposure. The evidence supports that the surface transformed to AgCl based on the measured values of silver chloride controls of 0.86 - 0.88. Possible explanations for an average value slightly below the theoretical 1:1 Cl:Ag value are (A) previously reported X-ray damage effects or (B) the use of elemental RSFs with uncertainties of up to 10 %. [35, 36] Regardless, the XPS and XRD suggest that the

surface silver's chemistry on the SW exposed wound dressing was consistent with AgCl while the bulk material retained a fraction of silver in the zero valent state.

3.3 Transformations due to WF exposure

The AgNM wound dressing exposed to WF visually changed color from blue (in the pristine material) to dark gray/black (in the exposed material, SI Figure S1). The morphological changes observed by SEM were quite different with the WF exposure as compared to SW exposure. Qualitatively, the WF exposed wound dressing surfaces became more uniform, as characterized by decreased surface roughness and a dramatic decrease in the number of visible particles on the surface compared to the pristine material or the SW exposed material, as measured by SEM (Figure 1C, SI Figure S3D and S3E). While the surface still contained a small number of discernable particles in the nano range, the features were poorly defined and devoid of any large crystals such as those observed in the case of SW exposure. One potential reason for this change might be the presence of a thick surface layer of adsorbed BSA on the surface obscuring the imaging of AgNMs.

The elemental XPS findings corroborate the SEM findings regarding the presence of a thin layer of protein on the surface of the wound dressing. Indeed, there was an appearance of the N 1s region immediately upon WF exposure (Figure 3, SI Figures S8 and S9) which remained constant throughout the 7 day exposure. Consistent with the idea of a thin film of protein forming, the Ag 3d intensity was also significantly suppressed, at times by over a factor of 30 from the starting Ag levels (SI Figure S9). This is attributed to the attenuation of the Ag 3d photoelectrons through a <10 nm thick protein layer. Another way of tracking this protein layer formation is by monitoring the changes in the N:Ag ratio (Figure 4 right). The N:Ag ratio (Figure 4, right) increased rapidly over initial exposures prior to settling at a value of 5.45 ± 1.09 for WF exposed wound dressings. While not employed in our analysis due to differential charging issues, the carbon region also showed a significant increase in photoelectron intensity. The surface enhancement in [C] is consistent with the adsorption of protein on the surface, specifically BSA.

With respect to the AgNM chemistry on the wound dressing surface, XRD measurements again exhibited the loss of the silver oxide peak and the concomitant formation of AgCl; a zero-valent silver bulk phase component remained (see Figure 2B). EDS supported the formation of AgCl with the growth of a significant chlorine component (Figure 1C) after WF exposure. There was also a large contribution from sodium. For both SW and WF exposure, the presence of silver chloride formation at the wound dressing surface is likely due to direct conversion of the Ag_2O through a dissolution, precipitation and redeposition process initiated by the formation silver chloride complexes [15]. In total, the XRD and EDS findings were consistent with each other. The XPS results again demonstrated that there was the uptake of chloride at the surface (Figure 3 and SI Figure S8), however the overall Cl 2p intensity was significantly decreased. This is consistent with the depression in the surface silver signal consistent with the previously mentioned BSA adsorption. Another impact of the Ag signal suppression was weak emission of the Ag MNN, which made extracting chemical information in the form of α' values more challenging. Regardless, we were able to obtain adequate signal to noise and the α' value was

723.0 eV ± 0.8 eV for long WF exposures. The shift from the AgCl control and SW exposure samples resulted from lower signal to noise significantly impacting one of the AgMNN values measured, which was also evidenced by the large standard deviation (0.8 eV). Without the outlier, the average was closer to 723.3 eV, although with the large noise present, it was not feasible to attribute that value to Ag_2O of AgCl.

While the Cl:Ag ratio does not contradict our assertion that AgCl is forming due to WF exposure, it does not behave consistent with sweat observations. There is a sharp increase from the pristine Cl:Ag value of 0.039 ± 0.02 to an average value of 1.61 ± 0.09 for $\geq$ 6 h wound dressing exposures to WF. Clearly, the Cl:Ag ratio was significantly enhanced (by a factor of almost 2), suggesting that the surface was AgCl functionalized *and* that there are other unidentified Cl-containing species adsorbed to the AgNM surface or the protein layer, such as NaCl and $AgCl_x$ species. Additionally, there was an initial spike in both the Cl:Ag and N:Ag ratios for the WF exposed wound dressing well beyond the final steady state value. We attribute the initial spike in both of these ratios to the suppression of the Ag 3d signal at early times (t < 2h) (for RSF adjusted photoelectron intensities, see SI Figure S9) due to protein layer formation. However, the N 1s signal, which is related to the protein layer, remains relatively constant from 1h on (Figures S8 and S9), which suggests that there is no loss of the protein layer once formed. In contrast, the total Cl 2p and Ag 3d signal intensity increased (SI Figure S9), suggesting that there could be the uptake of complexed silver species at later times (t > 6h), either onto the adsorbed protein layer from already released silver or from silver released from the wound dressing surface onto the protein layer.

3.4 Evaluation of silver released into simulated solutions

ICP-MS was used to determine the amount of silver released during exposure into the 10 mL of simulated SW and WF and reported as a mass fraction of measured released silver to total silver in the pristine wound dressing, Ag_{rel}/Ag_{total} ($\mu g_{rel}/mg_{total}$). 5.3 mg +/- 0.41 mg of total silver per wound dressing specimen were measured, based on the total mass of the specimen and the measured mass fraction of silver in the wound dressing, (0.10 +/- 0.0059) g/g (m_{Ag}/m_{WD}). For simulated SW (Figure 5, inset), released Ag measured below the detection limit until 6 h when (0.37 +/- 1.3) $\mu g_{rel}/mg_{total}$ was measured. At the 168 h exposure, (1.5 +/- 2.6) $\mu g_{rel}/mg_{total}$ Ag was released. Exposure of the wound dressing to simulated WF resulted in significantly more released silver after 168 h, (58 +/- 11) $\mu g_{rel}/mg_{total}$. In conjunction with the observations of silver chloride formation (Figures 1-4), the low amount of silver released into SW suggests that after the surface silver oxide underwent dissolution, the Ag complexes precipitated and deposited onto available nanoparticle surfaces. Preliminary evaluation of the impact of adsorption to the container walls suggested that this would be a minimally contributing factor to the measured Ag in the media.

In contrast, WF solution promoted and retained more released silver at all exposure times. A possibility to explain the increase in released Ag is that the BSA sequesters or stabilizes the released silver species, reducing re-deposition on the wound dressing surface as AgCl, and results in additional release at longer exposures. This phenomenon has been demonstrated in previous studies where AgNMs decreased in size after exposure to BSA due to silver

sequestration.[37] Additionally, we conducted control tests on the release of silver from wound dressings to test the roles of each component in the WF and SW, namely BSA and chloride components, $X\mathrm{Cl}_y$. The data revealed roughly an order of magnitude increase in silver concentration released from a BSA/ $X\mathrm{Cl}_y$ solution compared to $X\mathrm{Cl}_y$. Release tests in BSA alone resulted in order of magnitude increase compared to BSA/ $X\mathrm{Cl}_y$ (release solutions at same concentrations as WF and SW), providing further evidence of the ability of BSA to retain released silver species in solution (Data not shown). BSA's capacity to sequester silver is consistent with the XPS findings which revealed an enhancement in the Ag 3d peak at long WF exposure times on the wound dressing's surface, suggesting an adsorption of silver species directly to surface or silver species associated with adsorbed BSA molecules.

Qualitatively, our findings are consistent previous studies where > 200 fold increase was observed in silver released from wound dressing into Iscove's modified Dulbecco's medium (IMDM) with human serum substitute over simple saline.[8] However, our study suggested a factor of 10 to 30 increase in released silver in a BSA containing chloride solution over simply chloride, a difference which will be expounded upon in the discussion. Further qualitative analysis of the silver released into BSA/ $X\mathrm{Cl}_y$ and $X\mathrm{Cl}_y$ controls was conducted to examine the physical nature of the released Ag profile using time-resolved acquisition mode ICP-MS. Qualitatively, the data exhibited signatures that could be representative of NPs present in both media. However, it is important to note that we cannot glean information regarding the chemical nature of the individual species without additional measurements, which made further experimentation and characterization of particle release by ICP-MS beyond the scope of this study. While we checked for additional particles released during the course of the study, we did not find any conclusive evidence [38].

3.5 Zone of Inhibition Testing

To evaluate the impact of chemical transformations on antimicrobial efficacy, ZOI testing was performed using *S. aureus* and *P. aeruginosa*. These bacteria were chosen for their commonplace occurrence in wounds, especially in burns for which the wound dressing is employed.[19] For *S. aureus*, the zone of inhibition was between 11.4 mm and 12.2 mm for all exposure scenarios (Figure 6A). While increased SW exposure did result in a larger zone of inhibition compared to the pristine wound dressing for all samples tested, the 168 h specimen was the only significantly higher data point. With respect to WF, no statistically significant change *or* qualitative trend in ZOI value was observed, although there was a slight increase in absolute ZOI value for all WF exposed wound dressings. The pristine synthetic SW and the pristine simulated WF did not result in a measurable ZOI. Furthermore, none of the supernatants from the SW or WF exposures resulted in a measurable ZOI. The lack of ZOI is presumably due to the low amount (or absence of) silver loaded onto the disks for these supernatants and controls.

For *P. aeruginosa*, the zone of inhibition was between 9.1 mm and 10.0 mm, suggesting the *P. aeruginosa* was more recalcitrant to Ag than the *S. aureus* (Figure 6B). Exposure for 5 s to synthetic SW resulted in the largest ZOI (diameter 10.01 mm) for the wound dressings, which was significantly larger than all other SW exposure conditions and the pristine sample. While the

data reflect a decrease in ZOI value after this initial exposure, the wound dressing exposed to 24 h and 168 h of SW exposure still had a larger ZOI than the pristine wound dressing, although only the former had a statistically significant difference. In contrast, as the WF exposure increased, the measured ZOI value increased before plateauing, with both 24 h and 168 h wound dressing samples having significantly larger ZOIs than the pristine wound dressing. Similar to *S. aureus*, the pristine synthetic SW, the pristine simulated WF, and the exposed solutions did not result in measurable ZOIs for *P. aeruginosa*.

4. Discussion

The diagram in Figure 7 summarizes the expected chemical transformations that AgNM wound dressings undergo upon SW or WF exposure based on the results of this study. Upon exposure to either simulated fluid, immediate loss of the silver oxide layer in the pristine wound dressing was observed (XRD based findings), likely a result of dissolution. Previous studies have attributed dissolution of Ag_2O in low or non-alkaline conditions to the dissolution of surface AgOH functionality[39] and further work suggested that Ag_2O remains stable only under extremely alkaline conditions [40]. This dissolution would still occur if the speculated Ag_2CO_3 were on the surface based on Ag_2CO_3 and Ag_2O bulk solubility constants (K_{sp}), 8.1×10^{-12} and 2.6×10^{-8}, respectively [39-42]. While these bulk values for K_{sp} may differ for nano sized particles, they provide a basis for comparison.

However, as previously mentioned dissolution is not the only process to occur. In the presence of high chloride concentration, the majority of any released ions will instantaneously form AgCl and precipitate on the surface of the textile under current conditions. Indeed, reported values demonstrate the low K_{sp} (1.8×10^{-10}) for AgCl verifying our assertion.[40] In the case of the SW, this is most easily seen in the development of silver chloride signatures in the XRD and XPS (Figures 2, 3) and elementally in the EDS and XPS (Figure 4, S9) on the surface of the wound dressing. This suggests the surface chemistry of the wound dressing will transform almost immediately after application to the patient and initial release will be more consistent with the AgCl than with the starting silver/silver oxide surface that is found in the wound dressing. Furthermore, the high [Cl^-] (roughly 86 mmol L^{-1} and 147 mmol L^{-1} for SW and WF, respectively) will drive the [Ag^+] even lower than if the wound dressings were in pristine DI water. Based on the ICP-MS analysis, the surface of the AgNM wound dressing released a small amount of silver, roughly 1.5 $\mu g_{rel}/mg_{total}$, suggesting the surface was quickly passivated by silver chloride and suppressed further release. This is consistent with previous studies where little dissolved silver was detected after the exposure of AgNPs to an artificial SW [43] and other saline solutions.[44] Indeed, the presence of free [Ag^+] should be dramatically reduced due to the high [Cl^-]. Previous reports support this finding and have modelled the decrease at excess Cl concentrations for the stoichiometric formation of AgCl. At higher Cl concentration, a gradual increase in soluble silver was predicted as a function of increased chloride[15] due to the conversion of AgCl to $AgCl_2^-$ and $AgCl_3^{-2}$.

WF exposed wound dressings also comprised AgCl at the surface with zero valent silver in the bulk, as demonstrated by XPS and XRD chemical data, respectively. However, the surface also formed a protein film on the surface and continued to process at longer exposures,

despite the passivating impact of surface AgCl formation, as evidenced by ICP-MS and XPS data. Specifically, relatively large amounts of released silver were detected in the wound dressing-exposed WF and the amount increased for at least the first 6 h of exposure. Together, the data demonstrates that the WF treated AgNM surface continues to process overtime, releasing more silver from the surface than in the sweat exposure scenario (Figure 5). One possibility is that this is a function of ligand promoted dissolution, where the BSA from the WF assists in the released of additional silver species after the wound dressing surface transformation to AgCl (XPS and XRD). Indeed, the BSA component of the WF has been previously noted to adsorb soluble silver species and particles [37, 45]. Interestingly, our findings suggest that 5.8 % +/- 1.1% of the total silver in the wound dressing was released in 7 days WF exposure, assuming minimal loss to container wall adsorption, significantly more than the 0.14% released by SW exposure. The WF studies are comparable to previous studies which reported 7% Ag released from the same wound dressing in human serum substitute (in IMDM) in 3 days [8]. However, the increased magnitude of silver release could be a function of different protein types as well as the use of IMDM which contains additional amino acids which also might stabilize released silver. Additionally, Rigo et al employed a wound dressing which did not appear to contain Rayon layers. This would result in less available silver in the current study and another source of silver adsorption, ultimately lowering the amount of release detected. Regardless, the results from the WF study suggest continued surface processing occurs long term resulting in increased silver release. Furthermore, the released silver was found to deposit on the protein film, resulting in elevated Ag levels at long WF exposures (Figure 4, SI Figure S9).

It is likely that the observed release of silver measured by ICP-MS (Figure 5) is not in the free ion form, rather it is stabilized by BSA, bound to Cl (either as AgCl or in another silver-chloro complex), and in particulate form. Separate control studies were conducted to qualitatively survey the Ag product distribution of the released Ag present in the solutions with time resolved ICP-MS measurements. The data exhibited signatures for particles present in all components of the simulated media (Data not shown). While the particles observed are speculated to be AgCl in composition, those measurements were not taken and may be the focus of future research. Regardless, the continued release of silver at longer exposures suggests that the wound dressing surface continues to evolve even after transformation to an AgCl surface due to the influence of BSA.

Because an evolving chemical distribution was observed in the simulated fluids, the relationship between Ag chemical form and antibacterial efficacy of the wound dressing was examined. As previously explained, the bacterial targets *S. aureus* and *P. aeruginosa* were examined as they are two highly prevalent bacterial strains found in burn wound infections, together accounting for over 40 % of the bacteria isolated from burn wounds.[19] The *S. aureus* ZOI for the pristine wound dressing was similar to the ZOI determined previously in work by Castellano, et al.[46] The *P. aeruginosa* ZOI for pristine wound dressing determined in this study was lower than previously found, though it should be noted that different bacterial growth conditions were used.[46] Interestingly, our results differ from work by Taylor, et al., which showed *S. aureus* was more recalcitrant to the wound dressing than *P. aeruginosa*, though a different strain of *P. aeruginosa* was used.[47] The disparity in results between the ZOI data

presented here and in other works is likely due to the qualitative nature of the test and differences in bacterial growth protocols, as previously noted by Duran, et al.[48] Thus differences in magnitude of ZOI between the bacterial strains found in our work and others should not detract from the overall results that demonstrate little difference between the exposed and pristine wound dressing samples upon comparison.

Overall, ZOIs for the wound dressing after modeled human use were comparable with those measured for the pristine wound dressing, suggesting that the antimicrobial efficacy is not hindered by the chemical transformations occurring during use. These results agree with work by Choi, et al which determined that AgCl nanomaterials inhibited *Escherichia coli* growth more than pristine AgNMs.[49] At a minimum, these results suggest that use of AgNM-containing wound dressings and the subsequent surface transformation of silver and Ag_2O to AgCl upon exposure to simulated human fluids does not decrease the bactericidal activity of the wound dressing. The similar antibacterial efficacy of the pristine and processed wound dressing samples may be due to the remaining Ag^0 in the wound dressing, though this was not examined in further depth here.

Better understanding of the transformations that occur during human exposure is necessary as these transformed products will be present in the AgNM textile upon disposal. Since recent studies suggest that textiles, such as wound dressings, retain most of their silver after use [24], it is reasonable to assume that these antimicrobial properties will remain intact upon disposal. Our findings will improve the predictive capabilities of understanding the impact of human use on AgNM in wound dressings and other textiles, providing improved chemical inputs for modeling the fate of wound dressings after use in environmental systems. The impact of these "after use" transformations due to environmental exposure and potential changes in antimicrobial activity will be the subject of future studies.

5. Conclusion

Here we show that chemical and physical transformations can occur in consumer AgNM-containing wound dressings after modeled human exposure scenarios including synthetic SW and simulated WF. Exposure to synthetic SW caused the formation of a layer of AgCl on the surface of the wound dressing that minimized release of silver from the surface of the material. In contrast, exposure to simulated WF also resulted in a AgCl layer formation, but also resulted in increased release of Ag species, which remained in solution/suspension due to stabilization by BSA. Attenuation of silver measured at the surface suggested the formation of a protein layer on the wound dressing. Silver continued to release in the WF system for at least 6h after exposure initiated. At longer exposures, silver was observed to redeposit on the protein layer. The surface transformation to AgCl did not prevent the material from retaining its antimicrobial properties. This is consistent a recent study suggesting AgCl could be employed as an antimicrobial agent [50]. Exposed wound dressings showed similar or larger zones of inhibition as compared to pristine wound dressings for two common bacterial wound colonizers. Therefore, chemical transformations during use may not prevent the wound dressing from having unintended environmental consequences after use and upon disposal. Increased knowledge of the

chemical transformations that AgNM-containing textiles undergo during their use is necessary to understand chemical products that are entering the environment upon disposal.

Acknowledgements

DE Gorka acknowledges funding and support from the National Academy of Science – National Research Council Postdoctoral Research Associateship Program. DEG and JMG thank Maureen Williams for useful conversation about XRD detection limits. Additional information regarding XPS analysis, FIJI Script for ZOI analysis and more is available in the electronic supplementary information. Official contribution of NIST; not subject to copyrights in USA.

References

[1] N.S. Tulve, A.B. Stefaniak, M.E. Vance, K. Rogers, S. Mwilu, R.F. LeBouf, D. Schwegler-Berry, R. Willis, T.A. Thomas, L.C. Marr, Characterization of silver nanoparticles in selected consumer products and its relevance for predicting children's potential exposures, Int J Hyg Environ Health 218(3) (2015) 345-57.
[2] T. Benn, B. Cavanagh, K. Hristovski, J.D. Posner, P. Westerhoff, The Release of Nanosilver from Consumer Products Used in the Home, J Environ Qual 39(6) (2010) 1875-1882.
[3] D. Cleveland, S.E. Long, P.L. Pennington, E. Cooper, M.H. Fulton, G.I. Scott, T. Brewer, J. Davis, E.J. Petersen, L. Wood, Pilot estuarine mesocosm study on the environmental fate of Silver nanomaterials leached from consumer products, Sci Total Environ 421-422 (2012) 267-72.
[4] P. Limpiteeprakan, S. Babel, Leaching potential of silver from nanosilver-treated textile products, Environ Monit Assess 188(3) (2016) 156.
[5] C. Marambio-Jones, E.M.V. Hoek, A review of the antibacterial effects of silver nanomaterials and potential implications for human health and the environment, J Nanopart Res 12(5) (2010) 1531-1551.
[6] C. Bianco, S. Kezic, M. Crosera, V. Svetlicic, S. Segota, G. Maina, C. Romano, F. Larese, G. Adami, In vitro percutaneous penetration and characterization of silver from silver-containing textiles, Int J Nanomedicine 10 (2015) 1899-908.
[7] K. Kulthong, S. Srisung, K. Boonpavanitchakul, W. Kangwansupamonkon, R. Maniratanachote, Determination of silver nanoparticle release from antibacterial fabrics into artificial sweat, Part Fibre Toxicol 7(1) (2010) 8.
[8] C. Rigo, M. Roman, I. Munivrana, V. Vindigni, B. Azzena, C. Barbante, W.R.L. Cairns, Characterization and evaluation of silver release from four different dressings used in burns care, Burns 38(8) (2012) 1131-1142.
[9] A.B. Stefaniak, M.G. Duling, R.B. Lawrence, T.A. Thomas, R.F. LeBouf, E.E. Wade, M.A. Virji, Dermal exposure potential from textiles that contain silver nanoparticles, Int J Occup Environ Health 20(3) (2014) 220-34.
[10] N. von Goetz, C. Lorenz, L. Windler, B. Nowack, M. Heuberger, K. Hungerbuhler, Migration of Ag- and TiO2-(Nano)particles from textiles into artificial sweat under physical stress: experiments and exposure modeling, Environ Sci Technol 47(17) (2013) 9979-87.
[11] S. Wagener, N. Dommershausen, H. Jungnickel, P. Laux, D. Mitrano, B. Nowack, G. Schneider, A. Luch, Textile Functionalization and Its Effects on the Release of Silver Nanoparticles into Artificial Sweat, Environ Sci Technol 50(11) (2016) 5927-34.

[12] C. Lorenz, L. Windler, N. von Goetz, R.P. Lehmann, M. Schuppler, K. Hungerbuhler, M. Heuberger, B. Nowack, Characterization of silver release from commercially available functional (nano)textiles, Chemosphere 89(7) (2012) 817-24.
[13] T.M. Benn, P. Westerhoff, Nanoparticle Silver Released into Water from Commercially Available Sock Fabrics, Environmental Science & Technology 42(11) (2008) 4133-4139.
[14] D.M. Mitrano, E. Rimmele, A. Wichser, R. Erni, M. Height, B. Nowack, Presence of nanoparticles in wash water from conventional silver and nano-silver textiles, ACS Nano 8(7) (2014) 7208-19.
[15] J.Y. Liu, D.A. Sonshine, S. Shervani, R.H. Hurt, Controlled Release of Biologically Active Silver from Nanosilver Surfaces, Acs Nano 4(11) (2010) 6903-6913.
[16] V. Vosmanska, K. Kolarova, S. Rimpelova, Z. Kolska, V. Svorcik, Antibacterial wound dressing: plasma treatment effect on chitosan impregnation and in situ synthesis of silver chloride on cellulose surface, Rsc Adv 5(23) (2015) 17690-17699.
[17] A.P. Adams, E.M. Santschi, M.A. Mellencamp, Antibacterial properties of a silver chloride-coated nylon wound dressing, Vet Surg 28(4) (1999) 219-225.
[18] X.Q. Chen, B.J. Hu, X.D. Xing, Z.L. Liu, Y. Zuo, Q. Xiang, Preparation of grafted cationic polymer/silver chloride modified cellulose fibers and their antibacterial properties, J Appl Polym Sci 132(25) (2015).
[19] C.G. Mayhall, The epidemiology of burn wound infections: then and now, Clinical Infectious Diseases 37(4) (2003) 543-550.
[20] E. Lombi, E. Donner, K.G. Scheckel, R. Sekine, C. Lorenz, N. Von Goetz, B. Nowack, Silver speciation and release in commercial antimicrobial textiles as influenced by washing, Chemosphere 111 (2014) 352-8.
[21] C.A. Impellitteri, T.M. Tolaymat, K.G. Scheckel, The Speciation of Silver Nanoparticles in Antimicrobial Fabric Before and After Exposure to a Hypochlorite/Detergent Solution, J Environ Qual 38(4) (2009) 1528-1530.
[22] L.S. Dorobantu, G.G. Goss, R.E. Burrell, Effect of light on physicochemical and biological properties of nanocrystalline silver dressings, Rsc Adv 5(19) (2015) 14294-14304.
[23] P.L. Taylor, O. Omotoso, J.B. Wiskel, D. Mitlin, R.E. Burrell, Impact of heat on nanocrystalline silver dressings. Part II: Physical properties, Biomaterials 26(35) (2005) 7230-40.
[24] R.J. Courtemanche, N.S. Taylor, D.J. Courtemanche, Initiating silver recycling efforts: Quantifying Ag from used burn dressings, Environmental Technology & Innovation 4 (2015) 29-35.
[25] J. Fabrega, S.N. Luoma, C.R. Tyler, T.S. Galloway, J.R. Lead, Silver nanoparticles: behaviour and effects in the aquatic environment, Environ Int 37(2) (2011) 517-31.
[26] E. Navarro, A. Baun, R. Behra, N.B. Hartmann, J. Filser, A.J. Miao, A. Quigg, P.H. Santschi, L. Sigg, Environmental behavior and ecotoxicity of engineered nanoparticles to algae, plants, and fungi, Ecotoxicology 17(5) (2008) 372-86.
[27] C.R. Walters, E.J. Pool, V.S. Somerset, Ecotoxicity of silver nanomaterials in the aquatic environment: a review of literature and gaps in nano-toxicological research, J Environ Sci Health A Tox Hazard Subst Environ Eng 49(13) (2014) 1588-601.
[28] Y. Yang, M. Xu, J.D. Wall, Z. Hu, Nanosilver impact on methanogenesis and biogas production from municipal solid waste, Waste Manag 32(5) (2012) 816-25.

[29] Y. Yang, S. Gajaraj, J.D. Wall, Z. Hu, A comparison of nanosilver and silver ion effects on bioreactor landfill operations and methanogenic population dynamics, Water Res 47(10) (2013) 3422-30.
[30] ISO, Textiles — Tests for colour fastness — Part E04: Colour fastness to perspiration, ISO 105-E04:2008, 2008.
[31] T.W. Canada, KM; Cowan, ME; Lindsey, BJ, Challenging silver-influence of extraction medium on the release of silver from commercial silver dressings, 2007.
[32] J.M. Gorham, R.I. MacCuspie, K.L. Klein, D.H. Fairbrother, R.D. Holbrook, UV-induced photochemical transformations of citrate-capped silver nanoparticle suspensions, J Nanopart Res 14(10) (2012).
[33] S.J. Underwood, J.M. Gorham, Challenges and approaches for particle size analysis on micrographs of nanoparticles loaded onto textile surfaces, NIST Special Publication 1200-22 (2017) 22.
[34] A.V. Naumkin, A. Kraut-Vass, S.W. Gaarenstroom, C.J. Powell, NIST X-ray Photoelectron Spectroscopy Database, NIST/Department of Commerce, https://srdata.nist.gov/xps/Default.aspx, 2000.
[35] C. Powell, M.P. Seah, Precision, accuracy, and uncertainty in quantitative surface analyses by Auger-electron spectroscopy and x-ray photoelectron spectroscopy, Journal of Vacuum Science & Technology A: Vacuum, Surfaces, and Films 8(2) (1990) 735-763.
[36] J. Sharma, P. Dibona, D.A. Wiegand, Xps Studies of the Photo-Decomposition of Agcl, Appl Surf Sc 11-2(Jul) (1982) 420-424.
[37] A.K. Ostermeyer, C. Kostigen Mumuper, L. Semprini, T. Radniecki, Influence of bovine serum albumin and alginate on silver nanoparticle dissolution and toxicity to Nitrosomonas europaea, Environ Sci Technol 47(24) (2013) 14403-10.
[38] D.E. Gorka, J.M. Gorham, Physical and Chemical Transformations of Silver nanomaterial-containing Textiles after use, Biotech, Biomaterials and Miomedical: TechConnect Briefs 2018 (2018) 154-157.
[39] T.P. Dirkse, The Silver Oxide Electrode, J Electrochem Soc 106(5) (1959) 453-457.
[40] T.E. Graedel, Corrosion Mechanisms for Silver Exposed to the Atmosphere, J Electrochem Soc 139(7) (1992) 1963.
[41] W.W. Harrity, The equilibrium of silver chloride, silver hydroxide, potassium hydroxide, and potassium chloride in queous solution at different temperatures and varying concentrations of potassium hydroxide: the calculation of the heat of the reaction, Montana State University-Bozeman, College of Letters & Science, 1933.
[42] S. Frazen, Solubility Product Constants. <http://www4.ncsu.edu/~franzen/public_html/CH201/data/Solubility_Product_Constants.pdf>, 2014 (accessed April 26.2018).
[43] J. Hedberg, S. Skoglund, M.E. Karlsson, S. Wold, I. Odnevall Wallinder, Y. Hedberg, Sequential studies of silver released from silver nanoparticles in aqueous media simulating sweat, laundry detergent solutions and surface water, Environ Sci Technol 48(13) (2014) 7314-22.
[44] R.B. Reed, T. Zaikova, A. Barber, M. Simonich, R. Lankone, M. Marco, K. Hristovski, P. Herckes, L. Passantino, D.H. Fairbrother, R. Tanguay, J.F. Ranville, J.E. Hutchison, P.K. Westerhoff, Potential Environmental Impacts and Antimicrobial Efficacy of Silver and Nanosilver-Containing Textiles, Environmental Science & Technology 50(7) (2016) 4018-4026.

[45] A. Gebregeorgis, C. Bhan, O. Wilson, D. Raghavan, Characterization of Silver/Bovine Serum Albumin (Ag/BSA) nanoparticles structure: morphological, compositional, and interaction studies, J Colloid Interface Sci 389(1) (2013) 31-41.
[46] J.J. Castellano, S.M. Shafii, F. Ko, G. Donate, T.E. Wright, R.J. Mannari, W.G. Payne, D.J. Smith, M.C. Robson, Comparative evaluation of silver-containing antimicrobial dressings and drugs, International wound journal 4(2) (2007) 114-122.
[47] P.L. Taylor, A.L. Ussher, R.E. Burrell, Impact of heat on nanocrystalline silver dressings. Part I: Chemical and biological properties, Biomaterials 26(35) (2005) 7221-9.
[48] N. Duran, G. Nakazato, A.B. Seabra, Antimicrobial activity of biogenic silver nanoparticles, and silver chloride nanoparticles: an overview and comments, Appl Microbiol Biotechnol 100(15) (2016) 6555-6570.
[49] O. Choi, K.K. Deng, N.J. Kim, L. Ross, Jr., R.Y. Surampalli, Z. Hu, The inhibitory effects of silver nanoparticles, silver ions, and silver chloride colloids on microbial growth, Water Res 42(12) (2008) 3066-74.
[50] Y. Kang, J.-Y. Jung, D. Cho, O. Kwon, J. Cheon, W. Park, Antimicrobial Silver Chloride Nanoparticles Stabilized with Chitosan Oligomer for the Healing of Burns, Materials 9(4) (2016) 215.

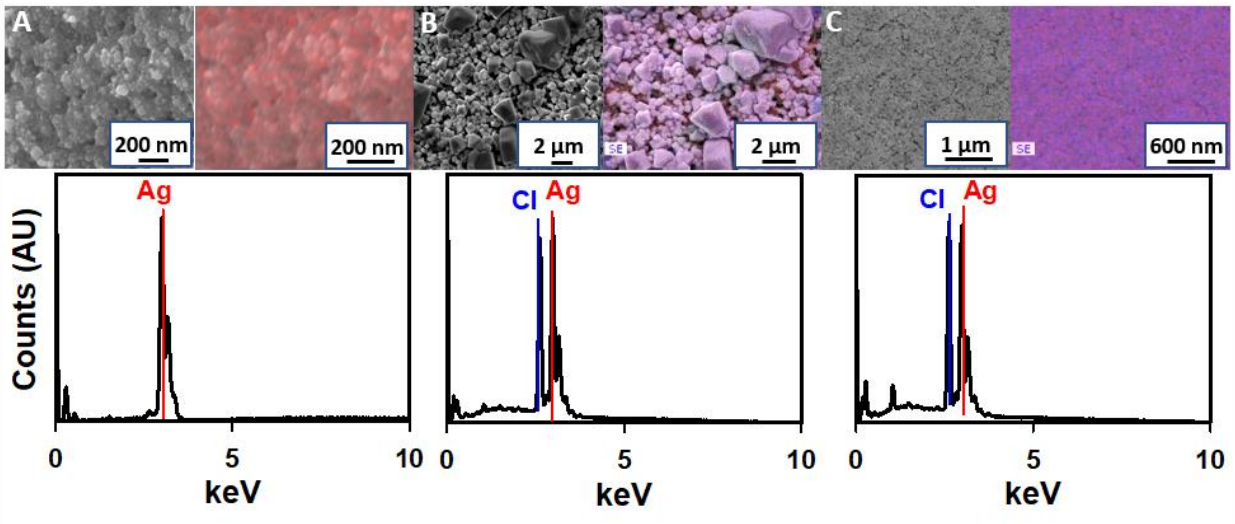

Figure 1: Scanning electron microscopy images, energy dispersive X-ray spectroscopy (EDS) maps, and EDS spectra of the wound dressing. A) Pristine wound dressing. Wound dressing after B) 168 h exposure to synthetic sweat and after C) 168 h exposure to simulated WF. [EDS Map Legend: Ag=red; Cl=blue; purple implies coincidence of Ag and Cl]

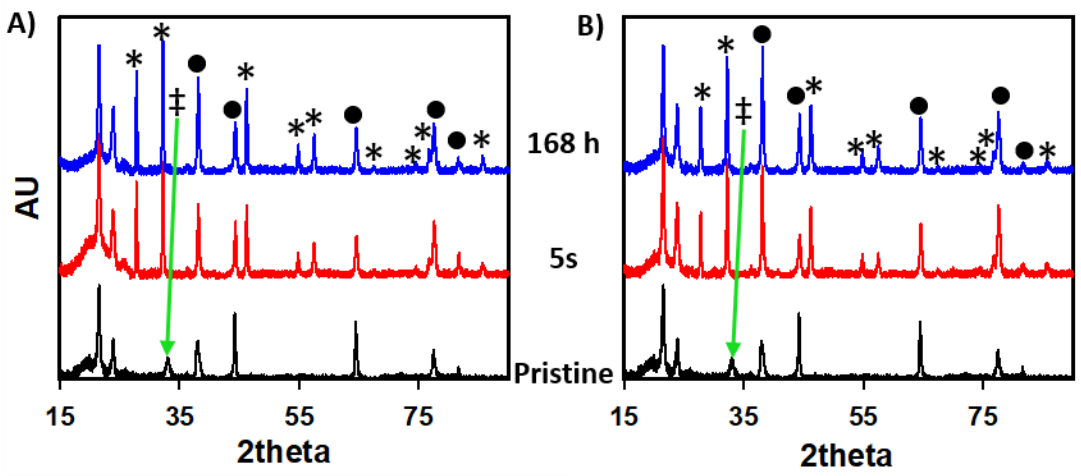

Figure 2: XRD spectra of the wound dressing before and after exposure to A) synthetic SW and B) simulated WF. Exposure of wound dressing results in the formation of AgCl, while the Ag_2O present in pristine wound dressing is lost. Note: ● indicates Ag^0, ‡ indicates Ag_2O, * indicates AgCl

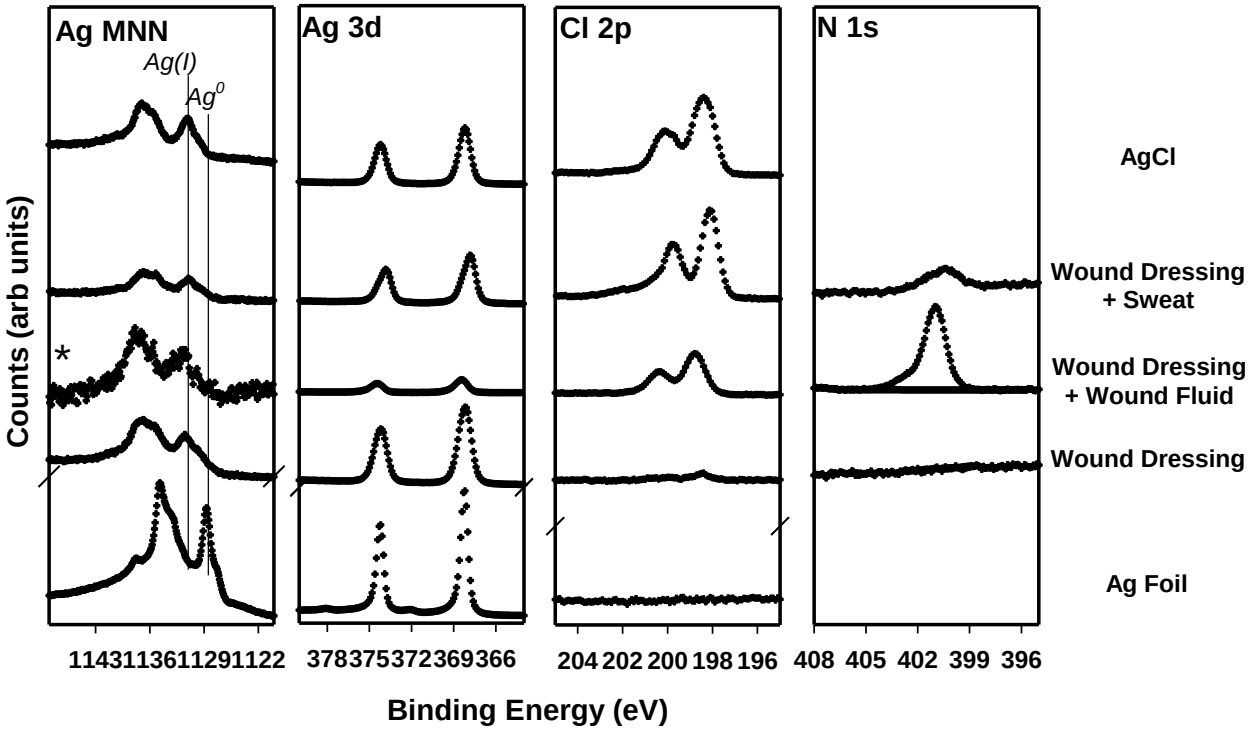

Figure 3: Representative X-ray Photoelectron Spectroscopy spectra of wound dressings (pristine and after exposure to SW or WF) and controls (Ag foil and AgCl) for the Ag Auger and photoelectron feature and Cl content. N signal was also acquired for the three wound dressings. The wound dressing specimens represent a pristine sample and 168 h of simulated human exposure (i.e. SW or WF). Note: For the wound dressing + WF specimen only, the Ag MNN transition is reflective of the sum of spectra from 4 different spots due to signal attenuation. All others are representative of one spot. *Additionally, the AgMNN plot was linearly background subtracted and subsequently multiplied by 30 for ease of viewing.

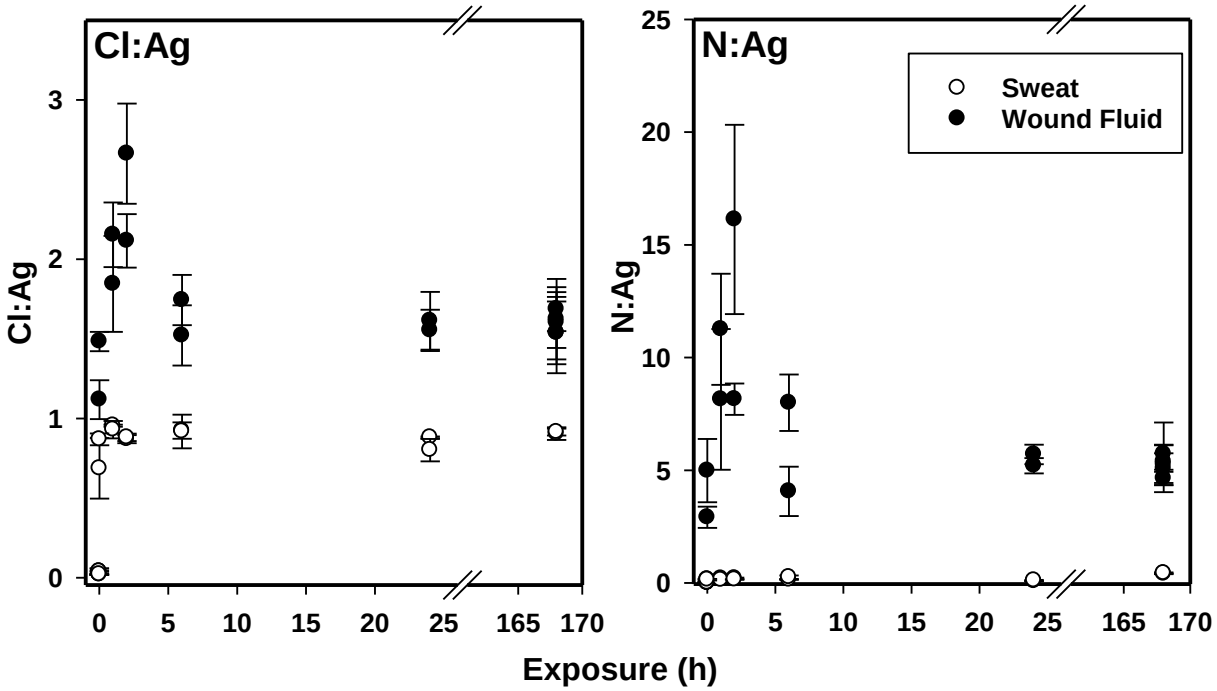

732
733 **Figure 4:** X-ray photoelectron spectroscopy analysis of all trial one wound dressings exposed to SW or
734 WF. Reported values (each data point) are the average and standard deviation of from 2 - 4 spots on
735 different parts of the trial one wound dressing. Additionally, the 168 h WF data reflects data from trial 2
736 and 3 to demonstrate reproducibility of the result. Average and standard deviation at 168 h for WF still
737 represent 2 - 4 spots.

738

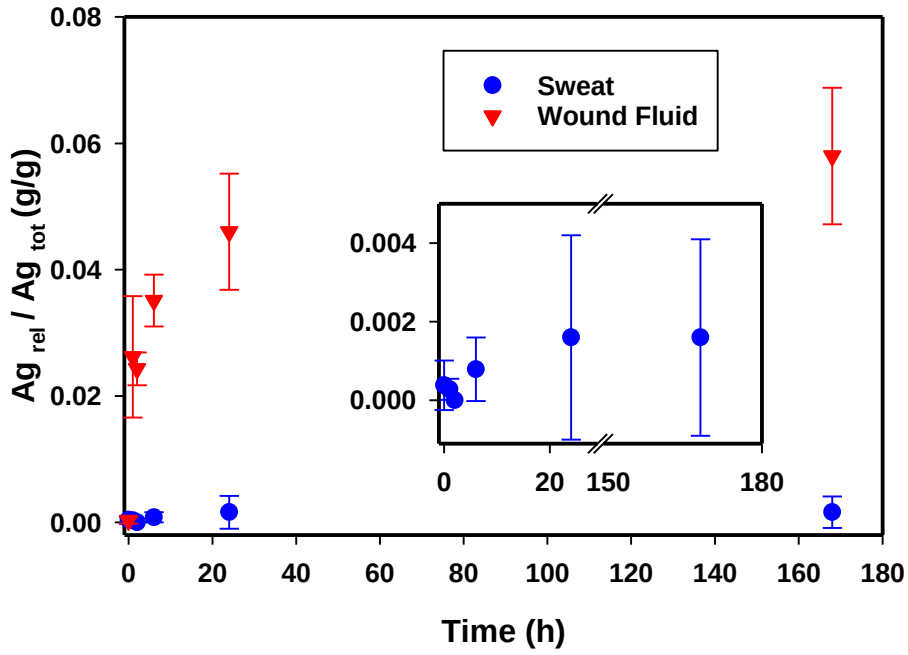

739

740 **Figure 5:** Inductively coupled plasma-mass spectrometry (ICP-MS) elemental analysis of SW and WF test
741 solution samples. *Inset* is a blow-up of SW exposure. Note: Values are shown as the mean of three
742 separate runs (i.e. five replicate per run) ± one standard deviation.

743

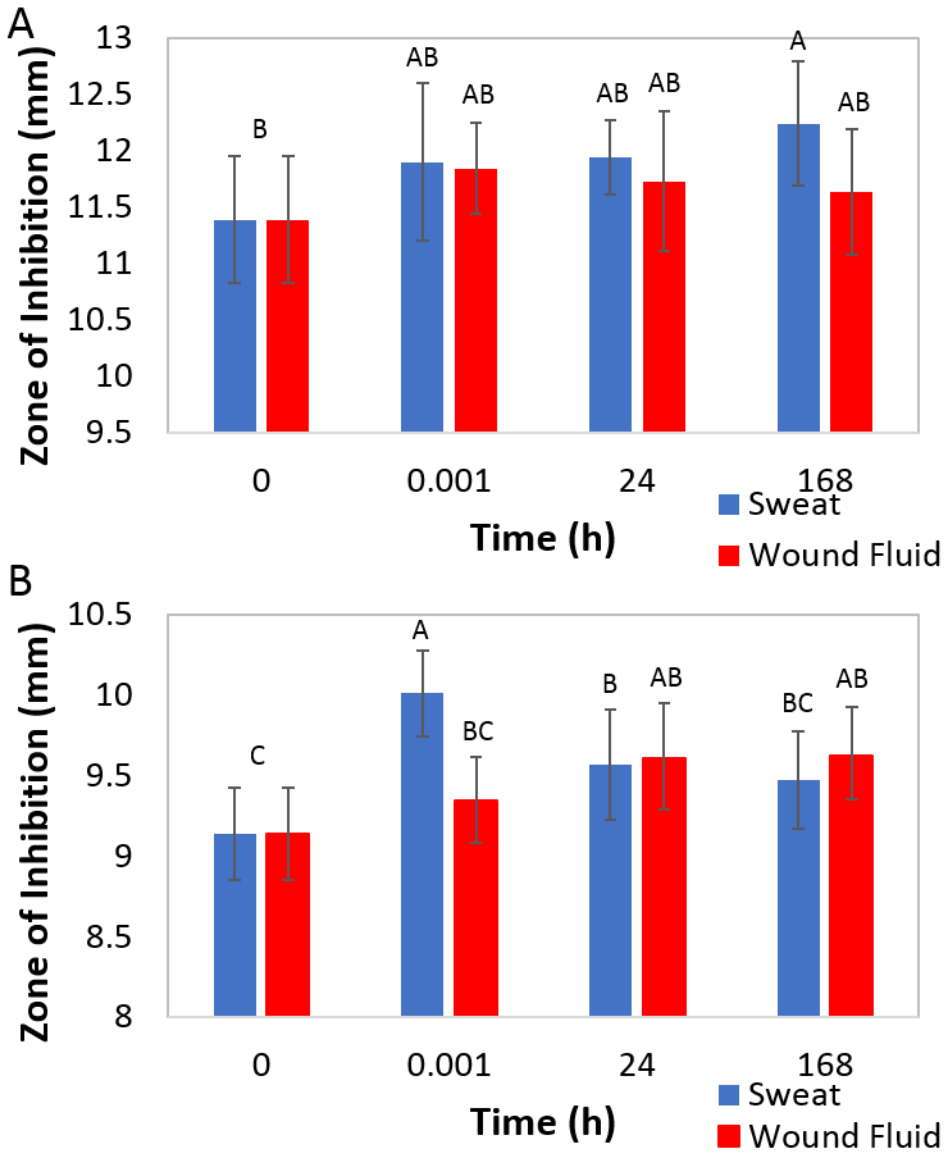

744

745 **Figure 6:** Zone of Inhibition analysis using A) *Staphylococcus aureus* and B) *Pseudomonas Aeruginosa* for
746 pristine, SW, and WF exposed wound dressing. Note: Values are represented as mean zone of inhibition
747 (n=9) ± one standard deviation. Different letters represent significant differences at $p < 0.05$ using a
748 Tukey HSD posthoc test.

749

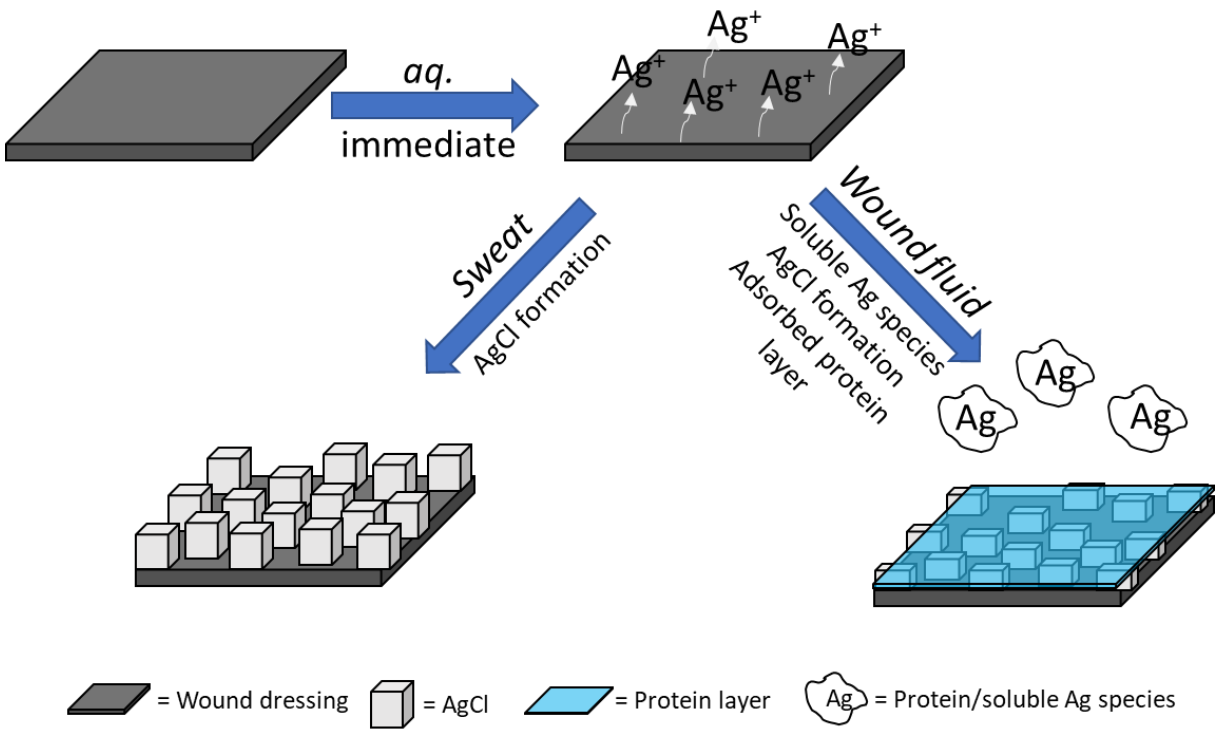

Figure 7: Scheme of theorized transformations occurring to nanosilver enabled textiles undergoing simulated human exposure in the current study.

Supporting information for:

Chemical and Physical Transformations of Silver Nanomaterial Containing Textiles After Modeled Human Exposure

Danielle E Gorka*, Nancy J. Lin, John M. Pettibone, Justin M Gorham*

National Institute of Standards and Technology, 100 Bureau Drive, Gaithersburg, MD, USA 20899

*daniellegorka@gmail.com; justin.gorham@nist.gov

For submission to NanoImpact

Visual appearance of Wound dressings before and after exposure

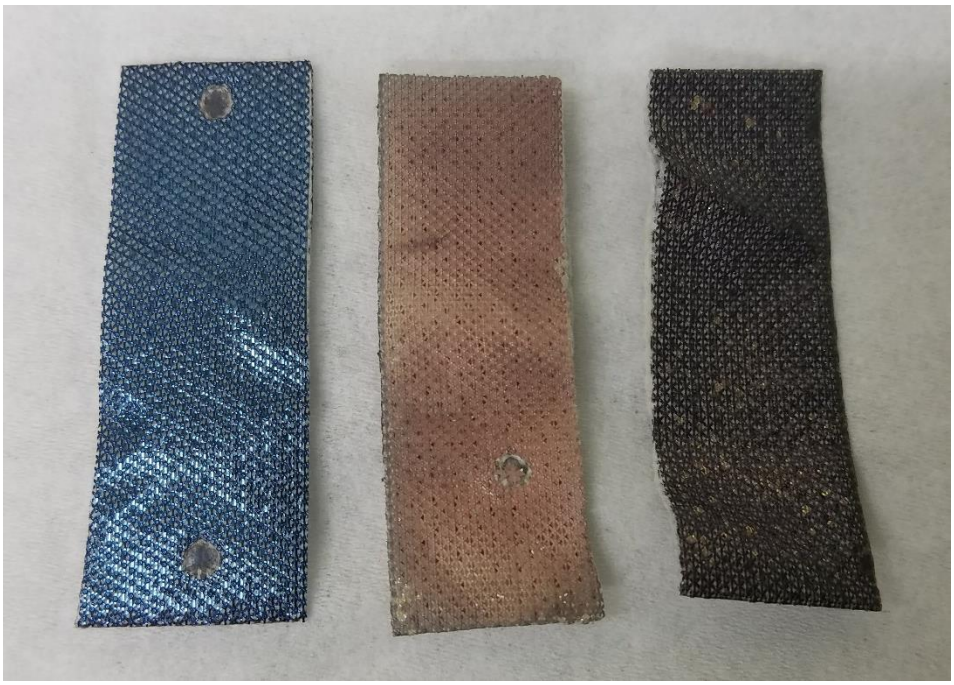

Figure S1. Images of the wound dressing. (Left) Pristine wound dressing, (Middle) Wound dressing after 168 h synthetic sweat exposure, and (Right) Wound dressing after 168 h simulated wound fluid exposure.

Core Characterization Techniques for measuring particle release

Exposure media was analyzed by UV-Visible (UV-vis) spectrophotometry using a PerkinElmer Lambda 750 spectrophotometer (Waltham, MA) to determine if particles were released from the wound dressing into the synthetic sweat and simulated wound fluid after exposure. UV-vis and DLS have been reported previously. Absorbance data was collected from 200 nm to 800 nm using a plastic microcuvette with a pathlength of 1 cm. Dynamic light scattering (DLS) using a Malvern Zetasizer Nano ZS (Westborough, MA) was performed to determine the sizes of any particles released into the exposure media. Bulk silver optical density and refractive index constants were used and scattering was measured at 173°. Exposure media samples were held at 23 °C for 180 s before the first run to equilibrate the temperature and held at that temperature during the run. For each sample, 8 measurements were made, each measurement consisted of 11 scans, and each scan was 10 s long.

Challenges and artifacts to avoid during XPS analysis of silver nanomaterials.

Several challenges and artifacts were known and observed during the characterization of the AgNMs on textiles by XPS. To start with, it has been established previously that X-ray exposure of silver halides, including AgCl, results in photodecomposition.[1] We tested the rate

of the photodecomposition using transformed and determined that the transformation occurred slowly, minimally effecting the results of our measurements of the sweat and wound fluid exposed wound dressings.

A second, unforeseen challenge resulted in the application of charge neutralization, or low energy electrons, to the surface of the oxidized starting wound dressing and the sweat exposed wound dressing. In both cases, the material transformed into a more metallic oxidation state. As a result, pristine wound dressings and those exposed to sweat could not be characterized by XPS using a charge neutralizer and therefore spots were selected that did not exhibit differential charging. With respect to wound fluid exposed wound dressings, the neutralizer was essential to dissipate charging for nearly all measurements and efforts were made to minimize exposure. Lastly, another result of the material employed was that the C 1s region would at times differentially charge when all other regions would not charge. We attributed this to the non-conductive nature of the polyethylene backing that the Ag/Ag_2O was loaded onto and assumed that this was a function of some heterogeneity regarding the completeness of the silver layer. As a result, we did not use the C 1s values in our elemental ratios or calculate elemental percentages.

Information on XPS background assignment and limited fitting for elemental analysis.

XP spectra were analyzed using CasaXPS (Teignmouth, UK) in efforts to obtain elemental ratio information and some qualitative oxidation state information. For all presented data, spectra were acquired for the Na 1s, O 1s, N 1s, Ag 3d, C 1s, Cl 2p, and Si 2p regions as well as the Ag MNN Auger electron transition. For analysis, Shirley backgrounds were applied to the Na, O, and Cl spectra, linear backgrounds were applied to the N and Si spectra, and a Tougaard fit was applied to the Ag spectra. While Shirley fits are the typical choice in our analysis, linear backgrounds have been found to be better at bisecting the noise for low surface concentration species and the same is true for the Ag region and the Tougaard fit.

Finally, to obtain elemental ratios, tabulated areas were corrected using elemental sensitivity factors provided by the instrument manufacturer.

ImageJ Script for assessment of ZOI regions

As mentioned in the main text, this script was based off a previously written macro, which was made for nanoparticle analysis[2] with selections of processing steps based on testing with a subsample of the images. The script operates by first defining pixel size to be 95 pixels/10 mm. The image is then converted from color (Figure S1A) to an 8-bit grayscale image. Contrast is enhanced using the automatically provided software values. Noise was reduced using "Gaussian Blur" with a sigma value of 2, while blurs everything with a radius of 3 pixels. A threshold was applied to the image including pixel intensities above a value of 190. In most images, these pixels were representative of regions devoid of bacteria, or the zone of inhibition (ZOI). Next in the script, we analyze the images for regions of interest using the conditions of a minimum area of 39 mm^2, a minimum circularity of 0.7, and including all holes (to include the sample) based on the brightest pixels defined by the thresholding values. We had the software generate an additional image reflective of the outlines of the identified ZOIs. We automatically saved the

processed image as the original file name with "_processed" (Figure S1B) tagged on at the end, and we saved the outlines image with the additional " outlines" tagged on. Lastly, the results table was saved using a filepath defined by the analyst under the filename Test.txt.

The files were processed using the batch processing tool in FIJI and loading the below text file containing the macro. All files in a given folder were processed. In the event that a ZOI was not calculated for a specimen, the result was checked to verify that no zone existed. If there was a problem with the thresholding for whatever reason, the image was reprocessed using the same macro. If the same result occurred, the area was approximated using the "Oval, elliptical" tool manually on the saved processed image.

Tox processing.txt

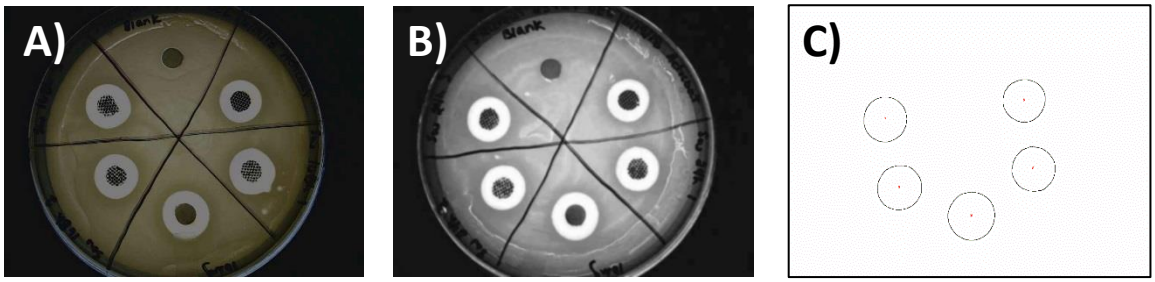

Figure S2: A) Image of Zone of Inhibition (ZOI) plate for representative run, B) image after processing, and C) ZOI areas defined by thresholding.

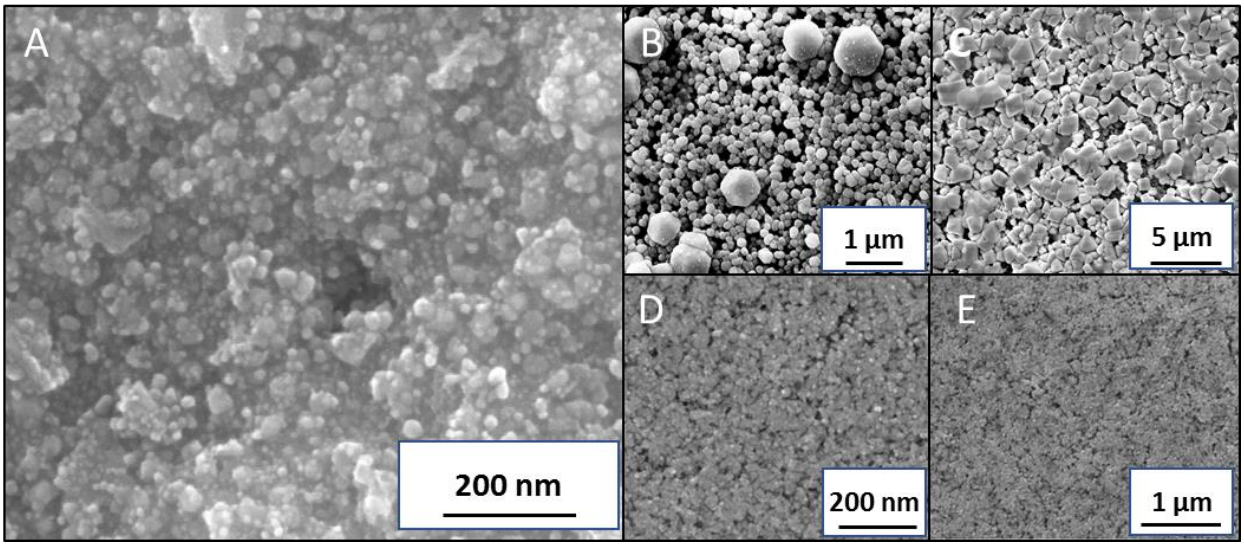

Figure S3: Scanning electron microscopy images of the wound dressing. A) Pristine wound dressing. Wound dressing after B) 5 s and C) 168 h synthetic sweat exposure and after D) 5 s and E) 168 h simulated wound fluid exposure.

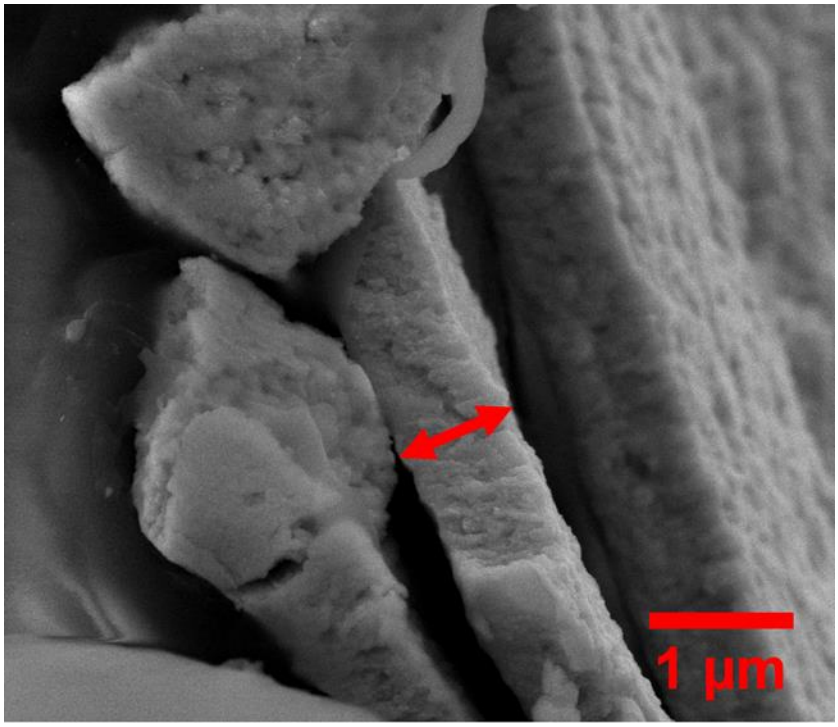

Figure S4: Scanning electron microscopy image showing the thickness of the silver layer on the wound dressing.

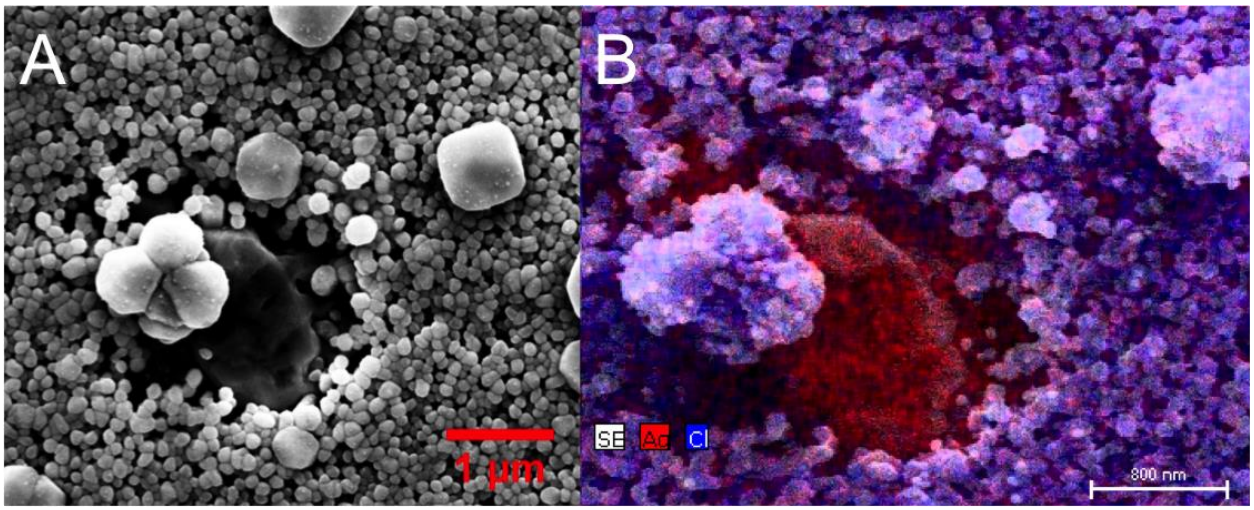

Figure S5: Scanning electron microscopy image (A) and energy dispersive X-ray spectroscopy map (B) showing the pitting of the silver layer on the surface of the wound dressing after sweat exposure.

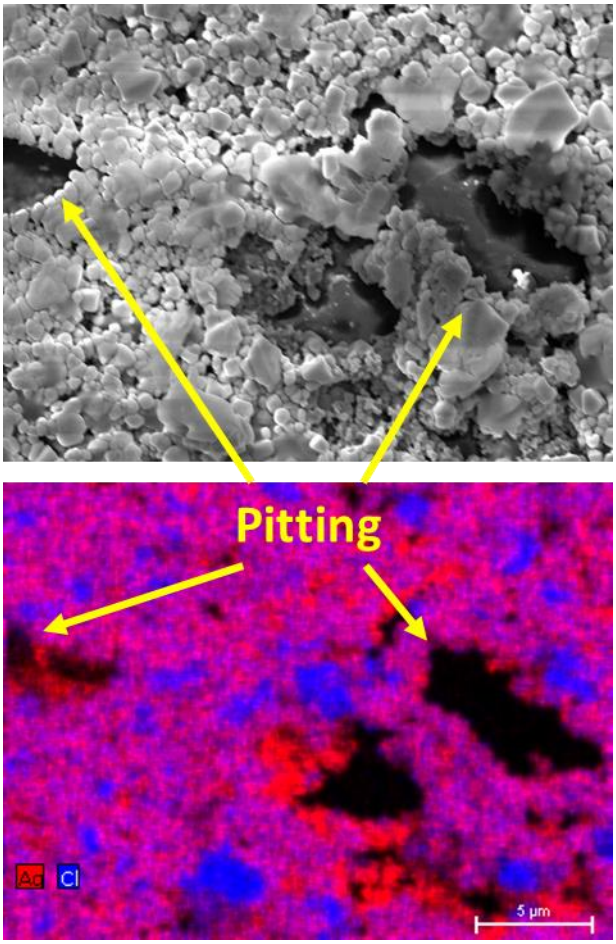

Figure S6: Scanning electron microscopy image (A) and energy dispersive X-ray spectroscopy map (B) showing the removal of the silver layer on the surface of the wound dressing after 168 h sweat exposure.

	α'	St. Dev.
silver foil	726.1	<0.1
silver chloride	723.5	0.1
silver oxide*	723.8	N/A
unexposed textile	723.3	0.1
sweat**	723.6	0.2
wound fluid***	723.0	0.8

*** 1 measurement**

**** 168 h all spots**

*****168 h r1 only**

862 **Table S1**: X-ray photoelectron spectroscopy α' values for various wound dressing samples and
863 controls.

864

865

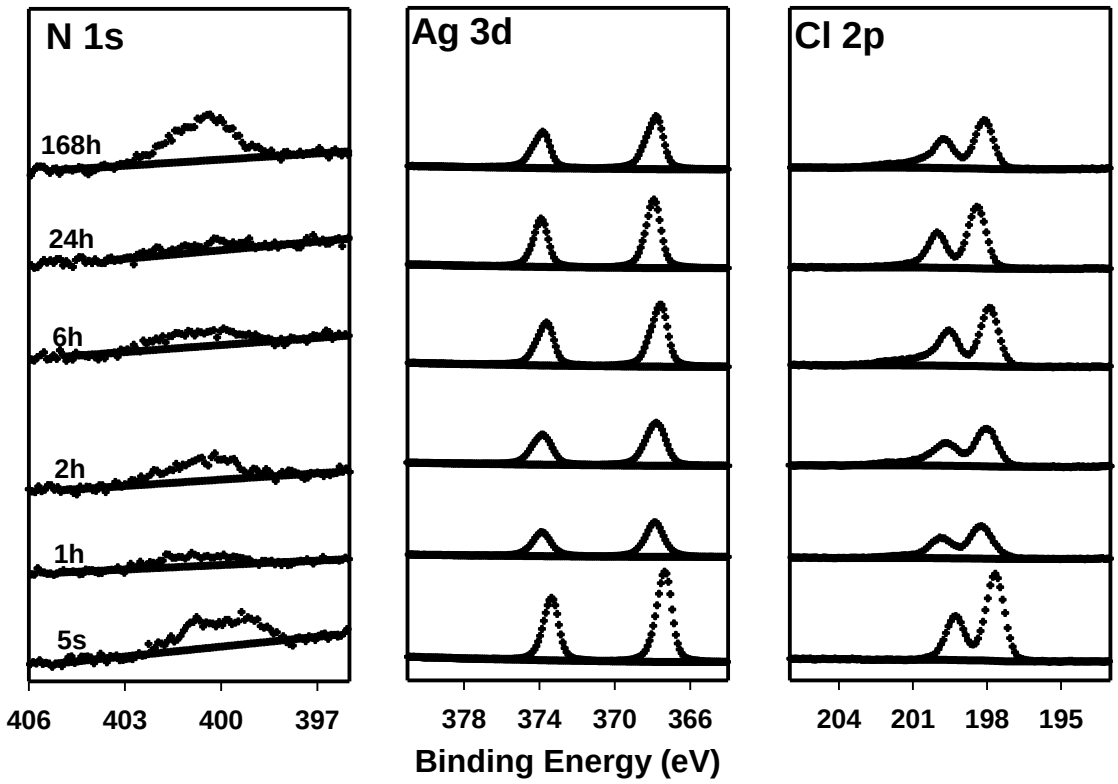

866

867 **Figure S7:** Stack plot of representative X-ray photoelectron spectra for the wound dressing
868 exposed to various durations of sweat exposure. Spectra is provided for the N 1s, Ag 3d, and Cl
869 2p regions.

870

871

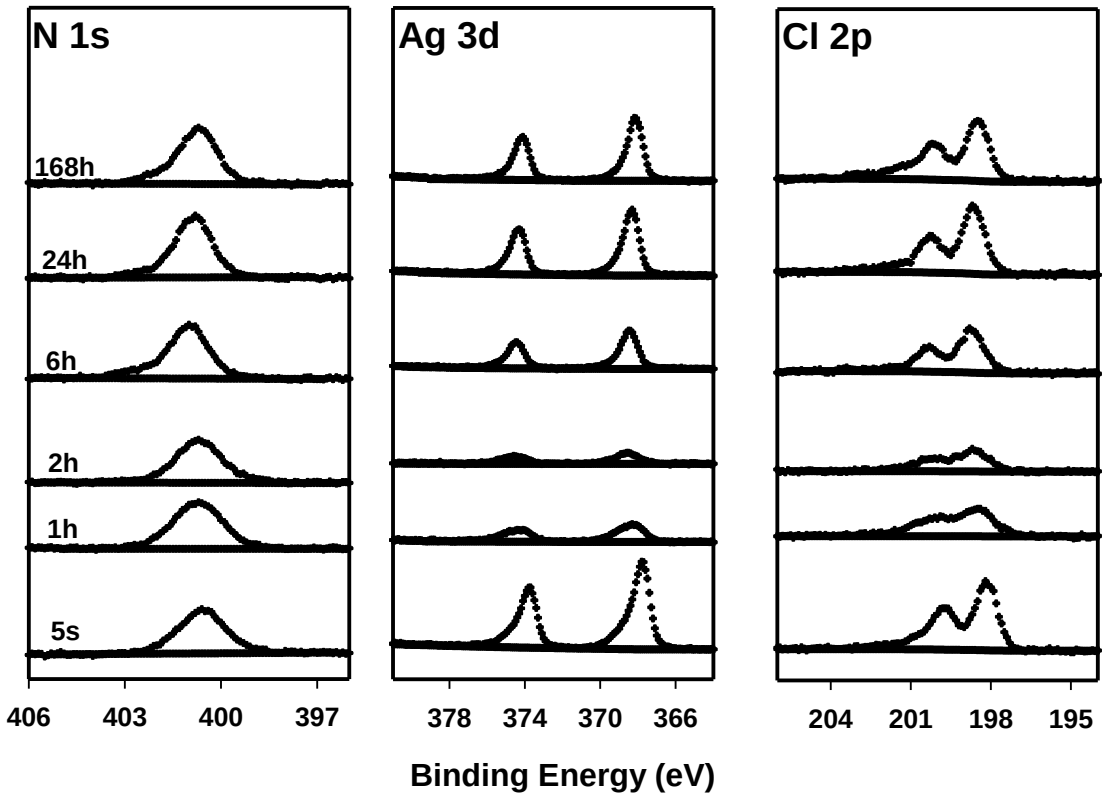

872

873 **Figure S8:** Stack plot of representative X-ray photoelectron spectra for the wound dressing
874 exposed to various durations of wound fluid exposure. Spectra is provided for the N 1s, Ag 3d,
875 and Cl 2p regions.

876

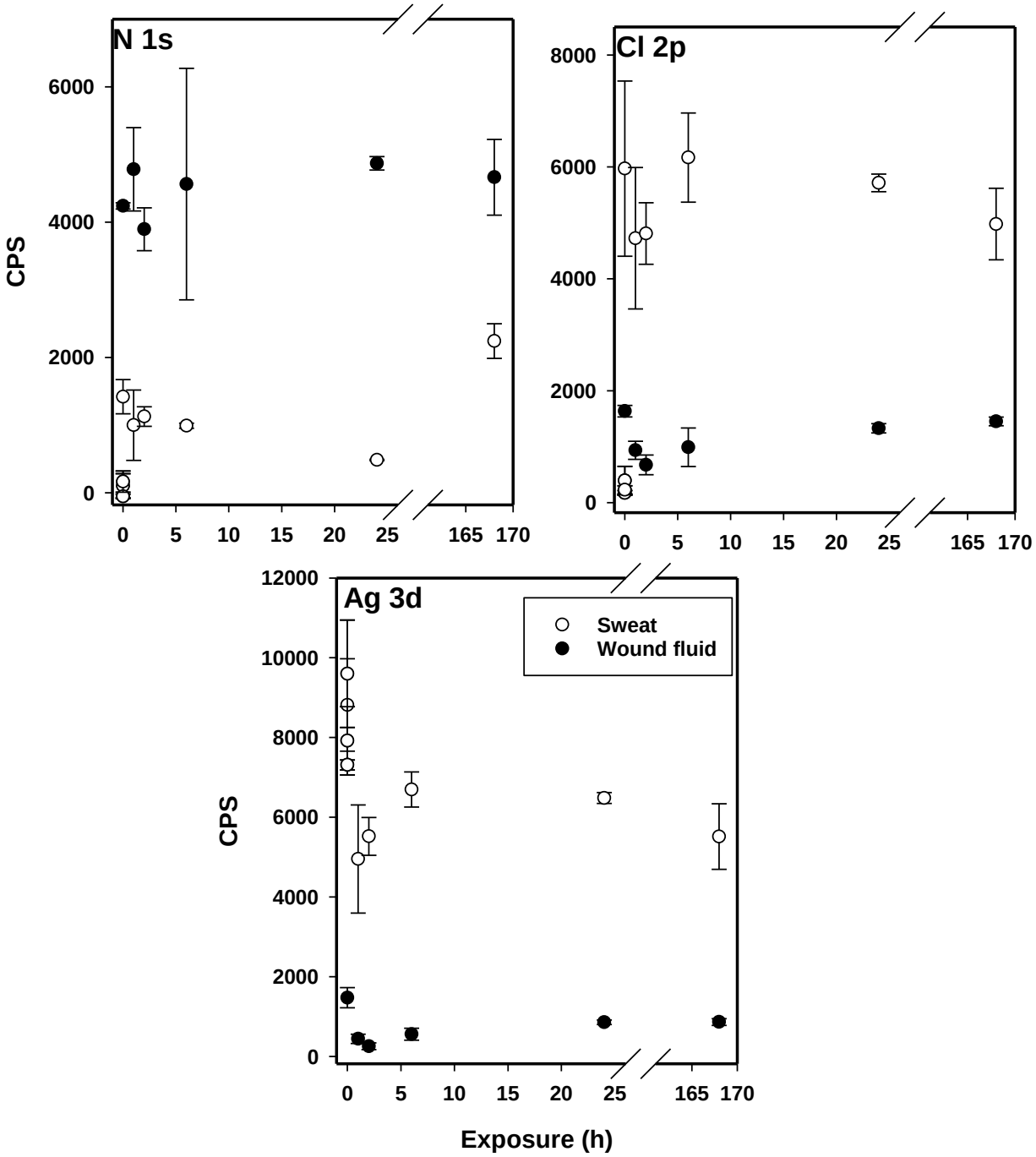

Figure S9: Relative sensitivity factor (RSF) adjusted photoelectron intensity of the N 1s, Cl 2p, and the Ag 3d regions for trial one. Each data point is the average and standard deviation of 2-4 spots from a specimen extracted from the trial one wound dressing.

References

[1] J. Sharma, P. DiBona, D. Wiegand, XPS studies of the photodecomposition of AgCl, Applications of Surface Science 11 (1982) 420-424.
[2] S.J. Underwood, J.M. Gorham, Challenges and approaches for particle size analysis on micrographs of nanoparticles loaded onto textile surfaces, NIST Special Publication 1200-22 (2017) 22.